TEMPERATURE VARIATION OF RAMAN SPECTRUM OF SODIUM CHLORATE

by 503

HARVEY LAWRENCE JOHNSTON, JR.

B. S., University of Missouri, 1967

A MASTER'S THESIS

submitted in partial fulfillment of the

requirements for the degree

MASTER OF SCIENCE

Department of Physics

KANSAS STATE UNIVERSITY
Manhattan, Kansas

1969

Approved by:

E Hathaway

Major Professor

TABLE OF CONTENTS

Introduction 1

The Raman Effect 3

The temperature Effects on the Phonon Spectrum 6

Crystal 9

Experimental Apparatus and Techniques 11

Discussion of Results 42

Summary and Conclusions 74

Appendix 77

Acknowledgements 80

References 81

INTRODUCTION

The harmonic oscillator model of matter was proposed as early as Newton[1] and was developed in the eighteenth and nineteenth centuries by many of the famous names in both physics and mathematics. Notable in this century are the contributions of Born[2] and Brillouin[3]. This model was a great success in describing the properties of solids. But there was one easily observed property, thermal expansion, that could not be explained by this model. Thus thermal expansion has been the traditional effect showing the harmonic model to be incomplete. Mie[4] and Grüneisen[5], early in the twentieth century, were the first to include anharmonic effects in their calculations. Since that time theoretical and experimental techniques have shown that anharmonic effects are present as perturbations on the harmonic model in most of the properties of solids. The understanding of anharmonic effects as of 1963 is reviewed by Leibfried[6,7].

One of the primary consequences of the harmonic oscillator model is the existence of lattice waves or phonons. The phonon frequencies are a direct measure of forces[8] between atoms and the associated elastic constants[9]. The half width of a phonon line is a measure of the phonon lifetime. The lifetime of a phonon depends directly on the interactions between phonons which results in part from anharmonicity. Thus a study of phonons is a very direct study of solids.

It is easiest to understand the success and failings of the harmonic approximation by examining the functional form of the potential energy. By requiring displacements of the atoms from their lattice sites to be small, the potential may be expanded in a Taylor series about the equilibrium point. With q_0 denoting the equilibrium point and η the

displacement from equilibrium position, the general coordinate can be written

$$q_i = q_{oi} + \eta_i \quad . \tag{1}$$

Thus the potential can be written

$$V(q) = V(q_o) + \sum_i \left(\frac{\partial V}{\partial q_i}\right)_o \eta_i + \frac{1}{2!} \sum_{ij} \left(\frac{\partial^2 V}{\partial q_i \partial q_j}\right)_o \eta_i \eta_j + \frac{1}{3!} \sum_{ijk} \left(\frac{\partial^3 V}{\partial q_i \partial q_j \partial q_k}\right)_o \eta_i \eta_j \eta_k + \ldots \quad . \tag{2}$$

The constant term can be set to zero by a proper choice of coordinate system and the linear term is zero because of the equilibrium conditions. In the harmonic approximation, the potential is truncated after the quadradic term. The succeeding terms are called the anharmonic terms. Most properties of solids can be described to a first approximation by the harmonic potential but a plot of a real potential, Fig. 1, shows deviation from the harmonic approximation. At low thermal energies (small displacements) the harmonic approximation is very good, while at higher energies the deviation becomes considerable. The anharmonic property most easily noted in Fig. 1 is thermal expansion as indicated by the shift of the equilibrium distance. As the thermal energy increases, the average distance between atoms increases and thus causes thermal expansion.

The temperature of a solid is relatively easy to control and measure. The study of thermal properties has been a useful method for the study of anharmonicity in matter. When considering anharmonic effects with respect to the phonon spectrum, it is to be expected that both the frequencies and phonon width will be a function of the temperature. Thus temperature

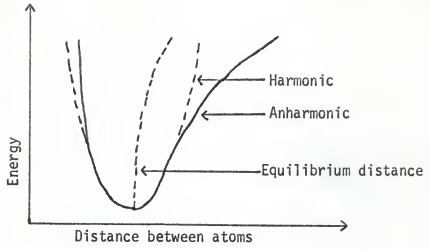

Fig. 1, Harmonic and Anharmonic Potentials

studies of phonon spectra may yield information on the anharmonicity of the crystal. Enough work has been done to show that the phonon spectrum is a function of temperature, but much of the work is qualitative and the studies are too few and incomplete to fully understand the results.

The Raman Effect

There are four main methods of studying phonons, i.e., infrared absorption and scattering of x-rays, neutrons, and visible light. Scattering of visible light, the Raman effect, has received great impetus with recent technical advances. The laser, new scanning monochromators, and photoelectric detection techniques have added greatly to the versatility, completeness, and ease of such studies using the Raman effect. The Raman effect was first reported by Raman[10] in 1927. Loudon[11] presents a review of the Raman effect and lists many references as of 1964.

The Raman effect is the scattering of light such that the energy of the incident light is changed by interaction with the phonons of the

substance. It can best be understood by assuming that the substance obeys the harmonic oscillator approximation, with q_k representing the normal coordinates expressed as

$$q_k = q_{ok} e^{i\omega_k t} \quad , \tag{3}$$

where q_{ok} is the amplitude and ω_k the frequency of the k^{th} mode. Consider the polarization, $\vec{P}$, of the material,

$$\vec{P} = \alpha \vec{E}, \tag{4}$$

or

$$\begin{pmatrix} P_x \\ P_y \\ P_z \end{pmatrix} = \begin{pmatrix} \alpha_{xx} & \alpha_{xy} & \alpha_{xz} \\ \alpha_{yx} & \alpha_{yy} & \alpha_{yz} \\ \alpha_{zx} & \alpha_{zy} & \alpha_{zz} \end{pmatrix} \begin{pmatrix} E_x \\ E_y \\ E_z \end{pmatrix} \quad , \tag{5}$$

where α is the polarizability and $\vec{E}$ is the effective applied electric field. The polarizability (neglecting the tensor character) may be expanded, for small displacements, in terms of the normal coordinates:

$$\alpha = \alpha^{(o)} + \sum_k \frac{\partial \alpha}{\partial q_k} q_k + \sum_{k,\ell} \frac{\partial^2 \alpha}{\partial q_k \partial q_\ell} q_k q_\ell + \cdots \tag{6}$$

$$= \alpha^{(o)} + \sum_k \alpha^{(1)} q_{ok} e^{i\omega_k t} + \sum_{k,} \alpha^{(2)} q_{ok} q_{o\ell} e^{i(\omega_k \pm \omega_\ell)t} + \cdots .$$

Thus if the electric field is periodic in time,

$$\vec{E} = \vec{E}_o e^{i\omega t} \quad , \tag{7}$$

the polarization, Eq. (4), can be written

$$\vec{P} = \alpha^{(0)} \vec{E}_0 e^{i\omega t} + \sum_k \alpha^{(1)} q_{0k} \vec{E}_0 e^{i(\omega \pm \omega_k)t}$$

$$+ \sum_{k,\ell} \alpha^{(2)} q_{0k} q_{0\ell} \vec{E}_0 e^{i(\omega \pm \omega_k \pm \omega_\ell)t} + \cdots \quad . \qquad (8)$$

The changing polarization presents an oscillating dipole which is the source of the scattered light. The first term in Eq. (8) causes Rayleigh scattering and is of the same frequency as the electric field. The second term will create first-order Raman scattering with a frequency, ω_k, less than and greater than the electric field frequency, ω. The succeeding terms are second and higher order Raman scattering. In general, the Rayleigh scattering is much more intense than first-order Raman scattering and the first-order Raman effect is much more intense than the second and higher order Raman scattering. The symmetry of the crystal lattice will allow only certain types of vibrations to be Raman active. That is, only certain lattice waves will give rise to a time varying polarizability. This limits the Raman scattering, $(\partial \alpha_{ij}/\partial q_k)$, tensors to a few forms for the various symmetry classifications. Loudon lists the possible Raman tensors for the various point groups associated with crystals. Examination of Eq. (5) shows that the polarization of the electric field in the incident light and the polarization of the scattered light, i.e. $\vec{P}$, will determine which component of the tensor is involved in the scattering process. Thus the scattered light will be polarization dependent. A very complete study of the Raman effect is presented by Nair[12].

Temperature Effects on the Phonon Spectrum

Maradudin[13] and Viswanathan[14] have authored theoretical papers concerning anharmonic temperature effects on the phonon spectrum. Maradudin's works are quite extensive but are not immediately applicable to experimental studies. Although Viswanathan's work is limited in a similar manner, it is possible to draw some experimental conclusions from it. He also applies his study directly to the Raman effect. Viswanathan[15] has shown that the self-consistent-field method of Hartree can be used in anharmonic problems by considering the anharmonic terms as perturbations of the harmonic oscillator. Thus, truncating after the cubic term, the potential can be written as

$$V = \frac{1}{2!} \sum_{i=1}^{N} \lambda_i q_i^2 + \frac{1}{3!} \sum_{ijk} \varepsilon_{ijk}\, q_i q_j q_k, \qquad (9)$$

where $q_1, q_2, \ldots, q_n$ (N = 3n-6) are the normal coordinates of a crystal with n atoms. The λ_is are the eigenvalues for the harmonic oscillator and the ε_{ijk}s are unknown anharmonicity constants. Using the Hartree method, Viswanathan derives the energy of the i^{th} normal mode as

$$\begin{aligned} W_{v_i}^{(i)} = {} & (v_i+\tfrac{1}{2})\, h\nu_i - \frac{5}{48} \frac{\varepsilon_{iii}}{\rho_i^3 h\nu_i} (v_i+\tfrac{1}{2})^2 + \frac{7}{60} + \frac{\beta_i^2}{8\rho_i^3 h\nu_i} \\ & - \sum_{m\neq i} \left[\frac{\varepsilon_{iim}\varepsilon_{mmm}}{4\rho_i\rho_m^2 h\nu_m} + \frac{\varepsilon_{mmi}\varepsilon_{iii}}{4\rho_i^2\rho_m h\nu_m} \right] (v_i+\tfrac{1}{2})(v_m+\tfrac{1}{2}) \\ & - \sum_{k\neq m\neq i} \sum_{i} \frac{(v_k+\tfrac{1}{2})}{4\rho_i\rho_m\rho_k h\nu_m} \left[\varepsilon_{iim}\varepsilon_{kkm}(v_i+\tfrac{1}{2}) + \varepsilon_{mmi}\varepsilon_{kki}(v_m+\tfrac{1}{2}) \right] \\ & - \sum_{m\neq i} \frac{\varepsilon_{iim}^2}{4\rho_m\rho_i^2 h\nu_m} (v_i+\tfrac{1}{2})^2 , \end{aligned} \qquad (10)$$

where $v_1, v_2, \ldots, v_N$ are integers denoting the degree of excitations of the different normal modes, ν_m is the m^{th} harmonic oscillator vibrational frequency,

$$\rho_m = \frac{4\pi^2 \nu_m}{h} ,$$

and

$$\beta_i = -\rho_i \sum_{m \neq i} \frac{\varepsilon_{mmi}(v_m + \frac{1}{2})}{\rho_m} .$$

Equation (10) shows that the energy of the i^{th} normal mode depends on the excitation, v_m, of the other modes with which it is interacting and the anharmonicity constants. Selection rules for first order Raman scattering limit the change of v_i to $(v_i \pm 1)$. Viswanathan assumes that most transitions are from the ground state, $v_i = 0$, to the first excited state, $v_i = 1$. This is true for low temperatures, but is certainly not the situation at higher temperatures. With these assumptions, Viswanathan states that

$$h\nu_i' = W_1^{(i)} - W_0^{(i)} = h\nu_i - \frac{5}{24} \frac{\varepsilon^2_{iii}}{\rho_i^3 h\nu_i} - \sum_m \left[A_m + B_m (v_m + \tfrac{1}{2}) \right] , \qquad (11)$$

where

$$A_m = \frac{\varepsilon^2_{iim}}{2\rho_m \rho_i^2 h\nu_m} ,$$

and

$$B_m = \frac{\varepsilon_{mmi}\varepsilon_{iii}}{4\rho_i^2 \rho_m \rho h\nu_i} + \frac{\varepsilon_{iim}\varepsilon_{mmm}}{4\rho_m^2 \rho_i h\nu_m} + \sum_{k \neq i,m} \frac{\varepsilon_{iik}\varepsilon_{mmk}}{4\rho_i \rho_m \rho_k h\nu_k} .$$

In the harmonic approximation, v_m can be regarded as the number of phonons in excited state having energy $h\nu_m$. The average value is given by

$$\bar{v}_m = \left[\exp(h\nu_m / kT) - 1 \right]^{-1} . \qquad (12)$$

Substituting Eq. (12) into (11)

$$h\nu_i' = h\nu_i - \frac{5\,\epsilon_{iii}}{24\,\rho_i^3 h\nu_i} - \sum_m (A_m + \tfrac{1}{2}B_m) - \sum_m B_m \left[\exp(h\nu_m/kT)-1\right]^{-1} . \quad (13)$$

At absolute zero, Eq. (13) reduces to

$$h\nu_{io}' = h\nu_i - \frac{5}{24}\frac{\epsilon_{iii}}{\rho_i^3 h_i} - \sum_m (A_m + \tfrac{1}{2}B_m). \quad (14)$$

It is interesting to note that even at absolute zero, $h\nu_{io}' \neq h\nu_i$. The shift from ν_{oi}' at temperature T is

$$h(\nu_{io}' - \nu_i') = h\Delta\nu_i = \sum_m B_m \left[\exp(h\nu_m/kT)-1\right]^{-1} . \quad (15)$$

The main observation to be made concerning Eq. (15) is that as the temperature increases, the frequency shift should increase. It is not possible to go beyond this because in general, the ϵ_{ijk}s are not known. However, at sufficiently high temperatures, the shift should be linear with temperature.

Another approach to the problem is to start with a form of Grüneisen's law, as given by the following expression:

$$\frac{\Delta\nu_i}{\nu_i} = -\gamma_i \frac{\Delta V}{V} . \quad (16)$$

Here ν_i is the harmonic frequency, $\Delta\nu_i$ the shift from ν_i, V and ΔV are the volume and change in volume, and γ_i is called Grüneisen's constant. It is often stated that γ is a function of frequency but not of temperature. Both frequency and volume can be measured, and it is of interest to determine how they both vary as a function of temperature. If it is assumed that a solid expands linearly with temperature, then

$$\Delta a = \alpha a_0 \, \Delta T, \tag{17}$$

or

$$\Delta V = 3\alpha \, V_0 \, \Delta T, \tag{18}$$

where α is the linear coefficient of expansion constant. Substituting Eq. (18) into (16) yields

$$\frac{\Delta \nu_i}{\nu_i} = -\gamma_i \, 3\alpha \, \Delta T. \tag{19}$$

In the Debye theory[16], the reduced frequency shifts, $\Delta\nu_i/\nu_i$, may be directly related to the variation of the Debye temperature Θ as a function of temperature. The Grüneisen constant may be defined as

$$\gamma = -\frac{\partial \ln \Theta}{\partial \ln V} = -\frac{V}{\Theta}\frac{\partial \Theta}{\partial V}.$$

From Eq. (18), the coefficient of expansion can be written as

$$\alpha = \frac{1}{3V}\frac{\partial V}{\partial T}.$$

Multiplying the Grüneisen constant by the coefficient of expansion yields

$$\alpha\gamma = \frac{1}{3V}\frac{\partial V}{\partial T}\frac{-V}{\Theta}\frac{\partial \Theta}{\partial V} = -\frac{1}{3}\frac{\partial \ln \Theta}{\partial T}$$

or

$$\frac{1}{\Delta T}\frac{\Delta \nu_i}{\nu_i} = -3\alpha\gamma = \frac{\partial \ln \Theta}{\partial T}. \tag{20}$$

No applicable theory of phonon half widths has been found by the author. Viswanathan assumes that thermal fluctuations of the volume elements could cause a statistical distribution of phonon frequencies and suggests a half-width dependence of the form

$$\nu_{\frac{1}{2}} = \left(\frac{kT\beta}{V}\right)^{\frac{1}{2}} \quad , \tag{21}$$

where k is the Boltzman's constant and β is the compressibility.

The rigor of the Grüneisen relation approach for both frequency shifts and half width is not very satisfying, but is at least suseptible to experimental testing.

Crystal

A cubic crystal with both covalent and ionic bonds which is easy to obtain or grow was wanted for this study. Sodium chlorate, $NaClO_3$, meets these criteria. Aravindakshan[17] has reported a complete study of the structure of $NaClO_3$, Fig. 2.

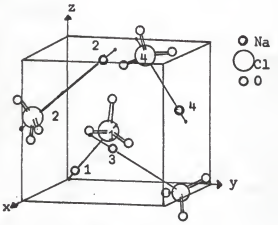

Fig. 2, $NaClO_3$ Unit Cell

The structure possesses the symmetry of the $T^4(P2_13)$ space group with 4 molecular units per unit cell. The cube edge has a length of a = 6.570 Å at 0^o C. Loudon lists the Raman tensors for such a cubic crystal as

$$R(A) = \begin{bmatrix} a & o & o \\ o & a & o \\ o & o & a \end{bmatrix}, \qquad R(E) = \begin{bmatrix} b & o & o \\ o & b & o \\ o & o & b \end{bmatrix}, \qquad R(E) = \begin{bmatrix} b & o & o \\ o & b & o \\ o & o & b \end{bmatrix},$$

$$R(F_x) = \begin{bmatrix} o & o & o \\ o & o & d \\ o & d & o \end{bmatrix}, \qquad R(F_y) = \begin{bmatrix} o & o & d \\ o & o & o \\ d & o & o \end{bmatrix}, \qquad R(F_z) = \begin{bmatrix} o & d & o \\ d & o & o \\ o & o & o \end{bmatrix}. \tag{22}$$

Thus phonons with A (non-degenerate) and E (doubly-degenerate) symmetries will be seen only when the polarization of the incident light is the same as the analyzed scattered light. The F (triply-degenerate) vibrations should be seen only when the polarizations are not the same. For example, refering to Eq. (5) and (22), the F_y vibration should be seen only with E_z and P_x or E_x and P_z.

Observations on frequencies involving different types of bonding were wanted because Narayanaswamy[18] in calcite, $CaCO_3$, and Kumari in $KClO_3$[19] and $NaClO_3$[20] have noticed that the behavior of the frequencies seems to fall into two groups, depending on the type of bond involved. The $CO_3^=$, ClO_3^-, etc. molecules have covalent bonds and the resulting vibrations are often referred to as internal modes. The covalent bonds are strong and it would be expected that small thermal energies would have little affect on them. The ionic bonds between the Na^+ and ClO_3^- ions are much weaker and thermal energies would be expected to have a stronger effect on frequencies involving changes in these ionic bonds. Kumari's study of $NaClO_3$ shows such shifts in the frequencies. However the numerical values in many of the early studies using mercury excitation sources and photographic recording have been shown to be in error. The study of $NaClO_3$ has been repeated and there is not good agreement with the earlier data.

EXPERIMENTAL APPARATUS AND TECHNIQUES

A laser Raman spectrometer with photoelectric detection was assembled and used for this experiment. The block diagram in Fig. 3 indicates the general nature of the experimental arrangement used for the Raman study.

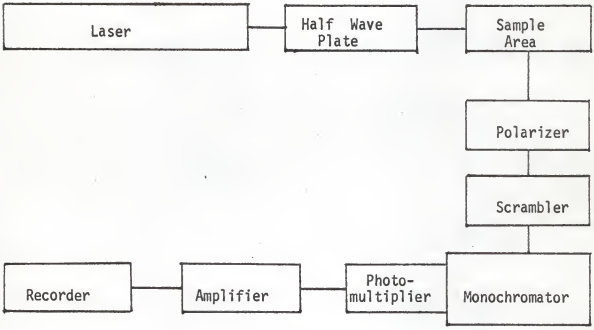

Fig. 3, Equipment layout

The laser has done much to advance Raman spectroscopy. The energy of the laser is concentrated in a narrow polarized beam of small band width as compared to the vapor-arc lamps. The variety of laser frequencies available permits selection to meet various conditions. Raman intensities are proportional to the fourth power of the frequency indicating the need for a high frequency source. However, many samples tend to fluoresce under high energy radiation. The cost and lifetime of different lasers place some limitations on the selection of exciting wavelengths. The laser used in these experiments was a Spectra Physics, Model 125, helium-

neon gas laser with a continuous output power of 50-70 milliwatts at 15,799 wavenumbers (cm^{-1}), i.e. 6328 Å. The normal Model 125 gas tube was replaced with a new cold cathode tube. The radio frequency (R.F.) excitation which increased the power in the old tube by approximately 100%, produced electronic noise in the amplified Raman signal. The R.F. excitation did not produce a significant gain in power with the new tube, and thus the R.F. excitation was unnecessary. The tube was also selected to have higher than average power for this model. Spex's "Ramanlogs"[21] lists the lines which a helium-neon laser emits in addition to the 6328 Å line. If these lines create a problem, an interference filter place in the beam before the sample will remove them. None of these lines were observed in this study.

In most Raman studies, it is of interest to know the polarization of the light incident upon the sample and the polarization of the light scattered into the monochromator. Since the laser beam is highly polarized, the polarization at the sample can be controlled by use of a half-wave plate. The half-wave plate used was mounted on the end of the laser and its 360^{o} rotation was calibrated in degrees. See Fig. 3. A polarization analyzer is placed between the sample and the monochromator. The analyzer was a polaroid filter mounted on the monochromator in front of the entrance slit. The polarizer could be rotated 360^{o}. It is best to place an optical wedge as a depolarizer between the analyzer and the monochromator slits. This eliminates the problem caused by the fact that transmission by a monochromator is polarization dependent. A quartz wedge was used to depolarize the scattered light.

A convenient notation has been developed to denote the combinations

of polarizations used. The notation is a(bc)d, where a is the direction of propagation of the incident light, b the polarization of the incident light, c the polarization of the scattered light, and d the direction of propagation of the scattered light. This notation is based on a laboratory fixed orthogonal coordinate system. Since $NaClO_3$ is cubic and the crystal axis are the same as the unit cell axis, the alignment of the unit cell axis with the laboratory system was not difficult. The geometry of the system limited the propagation of the incident light to the z axis and the scattered light to the y axis. Also the polarization of the incident light was limited to x and y and the scattered light to x and z. Thus the system was limited to the z(xx)y, z(xz)y, z(yx)y, and z(yz)y scattering configurations.

The efficient illumination of the sample and optimum collection of the scattered light is a difficult accomplishment. A monochromator is most efficient when the entrance slit is fully illuminated and the collimator mirror completely filled. The diameter of the laser beam is usually very small as compared to the length of the monochromator slit. Thus, for most efficient use, the axis of the laser beam should be along the slit length. Most monochromators have their slits vertical. Thus, the laser beam should enter the sample in the vertical direction or the image should be rotated before it reaches the slit. The former method was used in this instrument. A mirror was used to deflect the beam from the horizontal laser upward to the sample. This also permitted a compact arrangement.

The illumination system used with this instrument involves focusing the laser beam into the sample and collecting the image at the monochromator

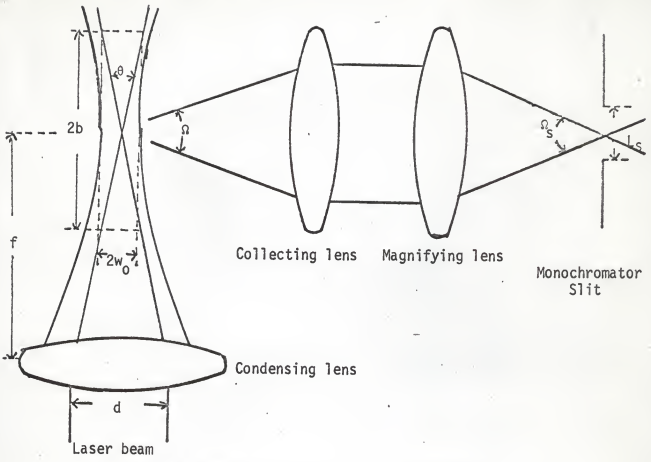

Fig. 4, Sample Illumination and Collection

slits. This allows the use of extremely small volume samples. The disadvantage of the decrease in the number of scattering molecules is offset by the increase in intensity in the small volume. The theory and experimental study of the problem of collecting scattered light and the optimum parameters has been performed by Benedek and Fritsch[22] and extended by Barrett and Adams[23]. Fig. 4 shows the geometry used. The focusing angle of the laser beam, θ, is well approximated by $\theta = d/f$, where d is the diameter of the laser beam and f is the focal length of the condensing lens. The parameter b is the length of the beam between the point of minimum radius, w_o, and the point at which the beam has a radius of $\sqrt{2}\ w_o$.

The beam does not focus to a true point because of diffraction effects and the minimum radius is given by

$$w_o = \frac{4\lambda}{\pi\theta} \quad , \tag{23}$$

where λ is the wavelength of the radiation. Thus the source of Raman scattering is effectively a cylinder of length 2b and diameter $2w_o$. Barrett and Adams show that there is a optimum value for θ and that it is bounded by

$$\frac{4\lambda M}{\pi w_s} \geq \theta \geq \left(\frac{16\lambda M}{\pi L_s}\right)^{\frac{1}{2}} \quad , \tag{24}$$

where w_s is the width of the slit, L_s is the length of the slit, and M is the magnification of the source image at the slit. The magnification is given by

$$M^2 = \Omega/\Omega_s, \tag{25}$$

where Ω is the solid angle the collecting lens subtends at the sample and Ω_s is the solid angle subtended by the magnifier at the slit.

Achieving optimum conditions turned out to be difficult. Using a helium-neon laser with a beam diameter of 2 millimeters and a monochromator slit length of one centimeter, Eq. (24) reduces approximately to

$$\frac{M}{w_s} \geq \frac{1}{4f} \geq .02\sqrt{M}, \tag{26}$$

where w_s is measured in microns and f is measured in centimeters. While the equipment was being assembled, it was not known what slit widths would be used. The best available collecting and magnifying system was an f/1.6, 16 mm projection lens system with a focal length of 4 cm. The dimensions

of the system required that the resulting magnification be approximately 8. A laser focusing lens of 2.5 cm focal length was also appropriate and practical for the system. Placing these parameters in Eq. (26) yields

$$\frac{8}{w_s} \geq .1 \geq .06 . \tag{27}$$

This indicates the system is optimum for slit widths of less than 80 microns The experimental conditions dictated the use of 40-160 micron slits so that fair optimization has been achieved. Larger magnification and/or a longer focal length condensing lens would have optimized the system for larger slit widths.

The major problem in aligning the instrument was the requirement that the laser beam intersect the optical axis of the monochromator, preferably at a right angle. A rough alignment could be achieved by placing a light inside the monochromator behind the entrance slit. With the slit open and the light on, the optical axis was defined by the light passing out the entrance slit and focused by the collecting lens. The mirror which changed the laser beam from horizontal to vertical was mounted on three points and furnished a fine adjustment of the position of the laser beam. By placing a card at the sample position and focusing the condensing and collecting lenses to form images near the sample position, a good alignment could be achieved by causing the images to coincide. Final alignment was made with the sample in place and the instrument registering a strong Raman peak. The mirror was then adjusted to obtain maximum signal. The focus of the laser needed to coincide with the point which the collector lens focused on the entrance slit to obtain maximum efficiency. This had to be adjusted for each sample and sampling condition. When aligning a sample for which the

settings were unknown, it was best to put the light inside the monochromator without the sample in place and use a card to adjust the settings until the images coincided. This was usually sufficient to obtain a Raman spectrum. Then the signal could be maximized with further adjustment.

The Raman spectrum is a collection of weak spectral lines which are shifts from a strong line incident upon the sample. The choice of monochromator to analyze the spectrum is initially dependent upon the detection system desired. With modern detectors, a photoelectric instrument is usually preferred.

The monochromator available for use in this instrument was a modified Perkin-Elmer Model 99-G double pass grating monochromator, Fig. 5.

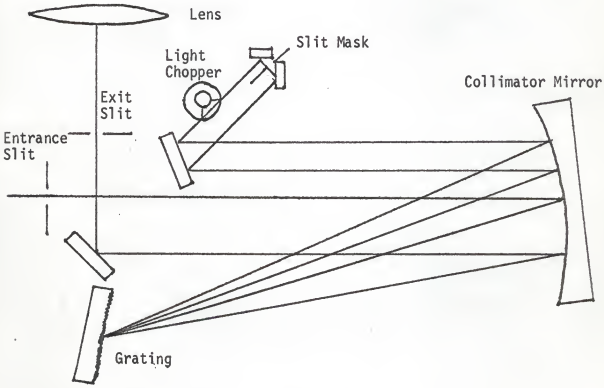

Fig. 5, Model 99-G Monochromator

The collimating and focusing element was an off-axis concave parabolic mirror. All mirrors had high reflectivity multi-layered dielectric coatings. The dispersive element was a 1440 lines per millimeter grating with an aluminum coating blazed for 5000 Å radiation. The entrance and exit slits were operated simultaneously by an external micrometer and curved slightly to correct for aberrations. The modifications of the Model 99-G were factory installed. They consisted of several additional baffles to cut down on light scattered inside the monochromator, the internal slit mask, and the dielectric coatings.

The double pass system was quite compact and the light passed the dispersive element twice, but it was very difficult to reduce stray light to levels comparable with more expensive systems with other configurations. The second-pass radiation was modulated by an internal chopper, while the first pass radiation appeared as a D.C. signal at the exit slit. A slit mask was placed at the first-pass focus of the collimating mirror to further cut down on stray radiation being chopped and reaching the exit slit as modulated radiation.

The various spectral components were made to move across the exit slit by rotating the grating. The width of the exit slit determined the width of the spectral band pass, and thus determined the resolution of the instrument. A lead screw and arm mechanism was used to rotate the grating. The coupling was such that the spectrum passing the exit slit was linear in wavenumber with respect to lead screw rotation. The lead screw could be rotated by hand or by a motor drive. Three speeds were available and a set of gears could be changed for further variation. An attachment on the lead screw opened a switch at regular intervals which controlled an event

marker on the chart recorder.

When a large flux of light was Rayleigh scattered into the monochromator by crystal imperfections, a number of peaks were found in the spectrum which could be mistaken for Raman frequencies. These were principally grating ghosts[24]. They were identified by scattering light into the monochromator so that Raman scattering was not involved and examining the resulting spectrum. This method also would find the extraneous lines emitted by the laser if they are present.

Raman scattered radiation presented to the detector may range in power from that which is easily detected to that which is below the level of the best detection techniques available. Photoelectric detectors are gaining widespread use over photographic emulsions. There is a fundamental distinction between photoelectric and photographic detection. The photographic system is non-scanning and each spectral element is observed during the total time of observation, while the photoelectric system is usually a scanning device and each spectral element is examined for only a portion of the total observation time. Thus the photographic technique is best where the signal is very weak and long observation time is needed. Also any fluctuation in intensity would affect all spectral elements equally. However, photoelectric detection usually obtains equivalent data from a stable system and the linearity of response from a photomultiplier often makes its use preferable to photographic detection.

The ITT-FW 130 photomultiplier tube, Fig. (6), was used in the Raman spectrometer. The S-20 photocathode used has the highest quantum efficiency presently available in the visible spectrum. Quantum efficiency is the ratio of the electrons emitted by the cathode to the photons

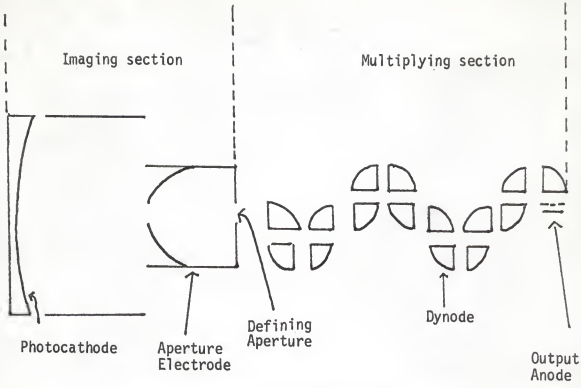

Fig. 6, ITT-FW 130 Photomultiplier Tube

incident. The current emitted by the photocathode is amplified by a series of 16 dynodes with an amplification of approximately 10^6. The ITT-FW 130 has several excellent features to reduce noise current not produced by photons on the cathode. The photomultiplier uses an anode guard ring to pass directly to ground most of the current resulting from the finite resistance of the glass insulation. Thermionic emission in the photocathode is a large source of extraneous electrons. The total number of thermionic electrons emitted will depend on the area of the photocathode and the temperature. Because of the lens after the exit slit in the monochromator, the actual area of the photocathode used is usually much smaller than most commercially available photomultiplier photocathodes. The ITT-FW 130 uses an electrostatic lens-aperture to limit the electrons reaching the first dynode to those originating in a small area of the photocathode. The size

and shape of the effective photocathode was built to match the exit slit of the monochromator used. The image of the slit and the cathode position were made to coincide by adjusting the position of the photomultiplier until the signal was a maximum. A Products for Research, Inc., Model TE-104TS Thermoelectric Cooler was used to hold the photocathode at -20°C to further reduce thermionic emission. A John Fluke Mfg. Co., Inc., Model 413 C High Voltage DC Power Supply supplied the 1800 volts DC photocathode-to-anode voltage recommended by the ITT-FW 130 instruction manual.

Two detection systems were considered for use in this instrument with the photomultiplier. The two systems were phase sensitive amplification and electron pulse counting. At low light levels, the signal from a photomultiplier consists of electron pulses correlated with the photons striking the photocathode. Thus pulse counting is often called photon counting. The number of counts per unit time is a measure of intensity and thus the spectrum can be scanned by determining the number of pulses in prescribed time intervals. This system has the advantage of being able to detect very weak signals since most forms of noise can be discriminated against. Thermionic emission by the photocathode is one exception, but it can often be minimized as previously discussed. Photon counting cannot be used at medium to large light signals because of the large number of counts per unit time involved.

The phase sensitive system was chosen for this instrument. This choice was dictated by the fact that a double pass monochromator was used. Some first pass radiation and other stray light would reach the photomultiplier and a photon counting system could not discriminate against them. The amplifier system used was a Princeton Applied Research, Model

HR-8 Precision Lock-In Amplifier, Fig. 7. The signal is amplified first by a low-noise, wide-band preamplifier, and then increased in level again by a moderate bandwidth amplifier tuned to the modulation frequency. The heart of the system is a phase sensitive detector. It selects the component of the signal which matches the modulation of the second pass radiation in the monochromator in frequency and phase and rectifies the signal for further amplification while the other components were filtered out. The final component was a D.C. amplifier and a DC signal was presented to the recorder.

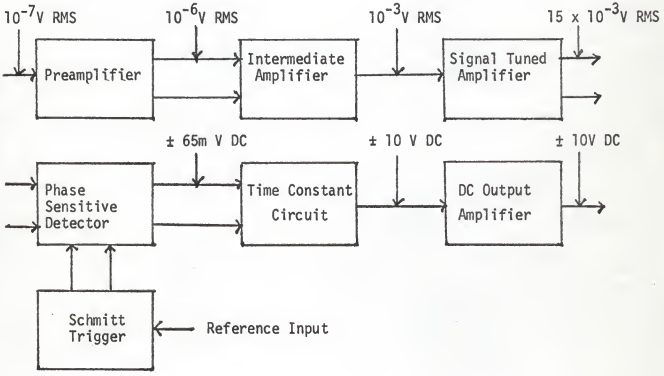

Fig. 7, PAR, Model HR-8 Amplifier

The reference signal was provided by a switch operated by a cam on the shaft of the chopper in the monochromator. The modulation was approximately 13 cycles per second, and fine adjustments in frequency and phase could be

made to obtain maximum signal.

The system had a wide range of sensitivity and a large selection of filter time constants. The full potential of the sensitivity selection on the PAR could not be used. The high sensitivity, requiring small monochromator slit widths, could not be used because the small amount of signal at that slit width would be a highly statistical and not reproducible signal. The photomultiplier output is a collection of very sharp spikes, and the PAR was designed to work with a more stable signal. If the slits were opened to use the lower sensitivities and as a result, the total flux reaching the photomultiplier was large enough, the photocathode would become temporarily damaged. Fortunately letting the phototube sit in the dark would allow the cathode to repair itself. This was normally not a problem except when large amounts of stray light reached the exit slit and/or the first pass radiation was extremely intense. The slits also could not be opened to give a strong signal because as the slits were opened, the monochromator resolution decreased. Thus there was constant conflict to stay away from the poor statistics of low signal and yet keep good spectral resolution.

A problem arose when a large flux of light reached the photocathode. The preamplifier of the PAR is designed to detect a voltage, while the photomultiplier emits electrons and thus a current, as a result the preamplifier would tend to overload and block the signal. The problem was solved by placing a large resistance across the input to the preamplifier.

The most common presentation of data from a scanning monochromator and amplifier is by a chart recorder. A Varian, Model G-14 Strip Chart Recorder was used for this instrument. The recorder had two chart speeds

and a very fast response time. A severe criticism of the Varian recorder was the poor arrangement for the event marker. The short response time, enabled a capacitor to be arranged to discharge a pulse into the pen drive so that a spike was placed directly on the chart output. This is a standard procedure on many recorders. The pulse was triggered by the switch on the lead screw on the monochromator. Using this, the monochromator and event marker were calibrated against known spectral lines of several vapor lamps. It was found that the calibration could change slightly in time. This was thought to be a temperature effect. The different calibration curves were found to be approximately parallel. Thus one calibration curve and one point on the true curve was sufficient for the correction. The laser line provided a convenient reference point. Therefore at the start and finish of each spectral run, the slits were almost closed and the position of the laser line determined.

The instrument settings were determined by the type or quality of the data wanted and by the limitations of the instrument. The variable settings were the width of the monochromator slits, the speed of the wavelength drive, the sensitivity of the amplifier, the time constant of the filter, and the speed of the chart drive. The easiest to set was the chart speed. The drive had two motors with a 5-to-1 ratio. The high speed was used when accurate measurements were wanted. The data was spread out over a longer distance and thus inherent measurement errors were minimized. The slow speed was used to scan a broad region where great accuracy was not required. The sensitivity of the amplifier was determined by the height of the most intense portion of the spectrum to be scanned. This was done after the slit width was selected. The remaining three are

interdependent. A small slit width is needed for good resolution, but small slit widths mean low power and relatively large amounts of random noise. This requires a long time constant to smooth out the random noise. A slow drive speed was required so that the change in true signal was small during one time constant period and would not be averaged out. For weak signals, the instrument was limited by the slowest monochromator drive speed. Thus the time constant had to be short enough to prevent loss of signal but long enough to remove as much noise as possible. If the resulting signal was so bad that respectable data could not be achieved because of the noise, the slits had to be opened. For scattering near the exciting line, much of the noise was associated with the Rayleigh scattering. Thus the perfection, preparation, and position of the sample greatly affected the quality of the data.

The various combinations of the polarization of the laser beam and analyzer setting result in different spectra. Four combinations are shown in Plates I and II. The peaks are indexed using the values reported by Ananthanarayanan[25]. The polarization dependence of some of the phonon peaks is readily observed. The phonons to be studied were selected to be internal and external modes with a minimum possible spectral overlap and with appreciable intensity. The z(xx)y setting allows both the A and E phonons to be studied. This also is the setting which yields minimum spectral overlap. For these reasons the following phonons were selected for study: 76, 151, and 205 cm^{-1} peaks were the external modes and the 487 and 940 cm^{-1} peaks were the internal modes. Plate III shows an expanded scan of the peaks studied.

EXPLANATION OF PLATE I

Survey spectra of $NaClO_3$ at room temperature for two different polarizations. The peaks are labeled in agreement with Ananthanarayanan[25].

Fig. 1: z(xx)y polarization.

Fig. 2: z(yx)y polarization.

	Frequency (cm-1)	Symmetry
A	70	E
B	83	F
C	103	F
D	123	F
E	131	A
F	179	E
G	482	E
H	487	F
I	627	F
J	933	-
K	936	A
L	966	F
M	984	F
N	1028	F

PLATE I

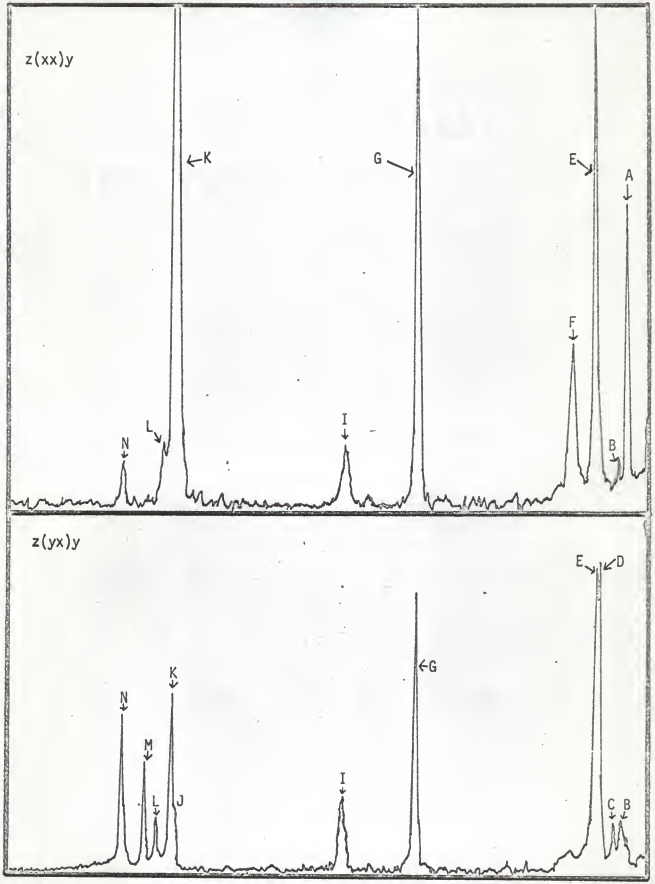

EXPLANATION OF PLATE II

Survey spectra of $NaClO_3$ at room temperature for two different polarizations. The peaks are labeled in agreement with Ananthanarayanan[25].

Fig. 1: z(yz)y polarization.

Fig. 2: z(xz)y polarization.

	Frequency (cm^{-1})	Symmetry
A	70	E
B	83	F
C	103	F
D	123	F
E	131	A
F	179	E
G	482	E
H	487	F
I	627	F
J	933	-
K	936	A
L	966	F
M	984	F
N	1028	F

PLATE II

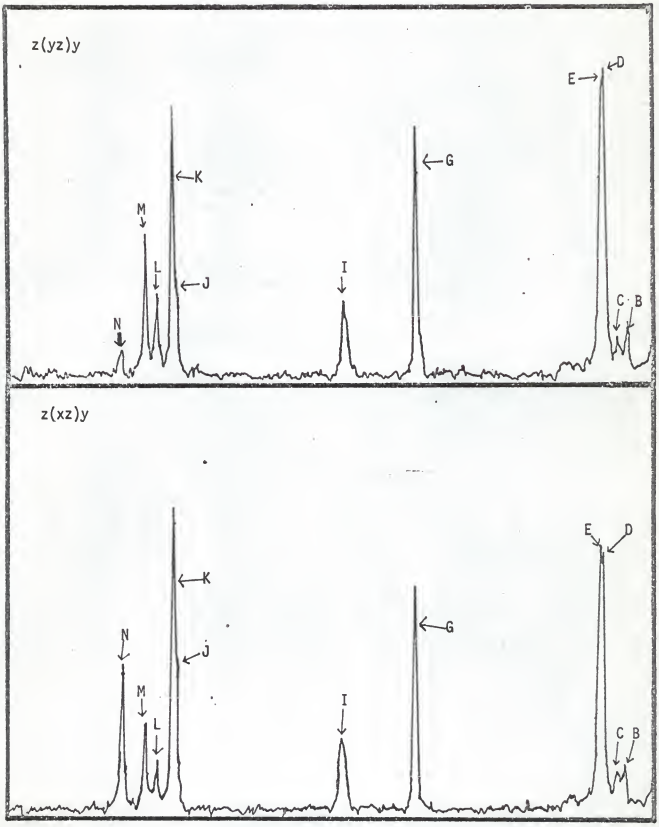

EXPLANATION OF PLATE III

A partial survey spectrum of $NaClO_3$ at room temperature for the z(xx)y polarization.

PLATE III

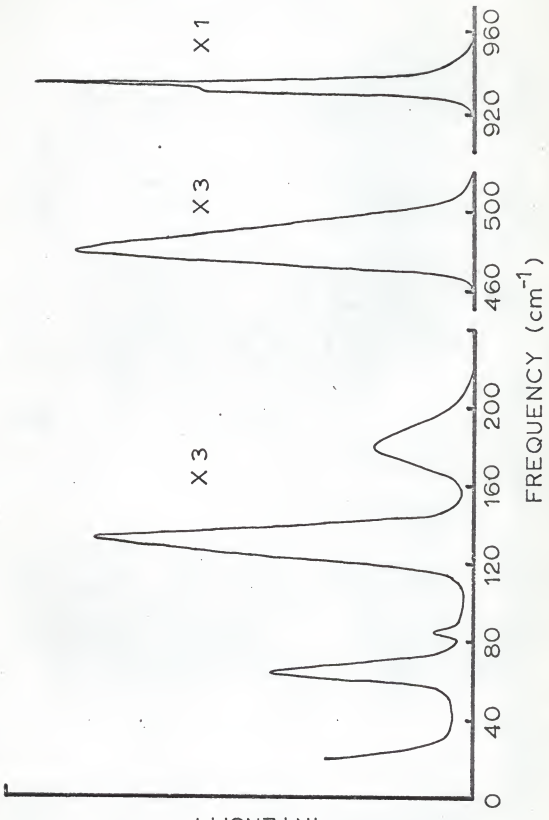
INTENSITY
0
40
80
120
160
200
460
500
920
960
FREQUENCY (cm^{-1})
X 3
X 3
X 1

The crystals were grown in this laboratory by colleagues of the author. The technique of growing the crystals consisted of cooling and evaporating saturated solutions. It was very difficult to grow crystals of large size and perfection. It was found that condition of the surface and interior perfection greatly affected the Rayleigh scattering of the laser beam. This was a problem when studying low frequency phonons since they then are superimposed on the wing of the Rayleigh scattered peak. It was found that minor surface imperfections could be removed by careful polishing with alcohol and very fine grinding compound. Care had to be taken that the crystal was not touched since the moisture from the hands is detrimental to the surface. For room temperature studies, the crystal was usually mounted on a crystal goniometer which allowed precise alignment.

A heater, Plate IV, was built for the high temperature portion of the study. The heater consisted of a copper rod wound with a nichrome wire heating element using Sauereisen cement as the electrical insulator. An iron-constantan thermocouple and John Fluke Mfg. Co., Inc., Model 803 B Differential AC-DC Voltmeter was used to monitor the temperature. An Athena, Model 63 Precision Proportional Temperature Controller was used to regulate the temperature. A platinum resistor was inserted into the copper rod and its resistance was monitored by the controller. An attempt was made to mount the crystal in a copper block inserted into the heater. The optics of the illumination system required that four of the six sides of the crystal be optically clear. Since the laser entered from below the crystal, the crystal could not rest on its base unless it was a large crystal. The crystal had to be held fixed since any movement would affect the focus of the lenses and might position the crystal to cause more in-

EXPLANATION OF PLATE IV

A diagram of the heater used for the studies above room temperature.

PLATE IV

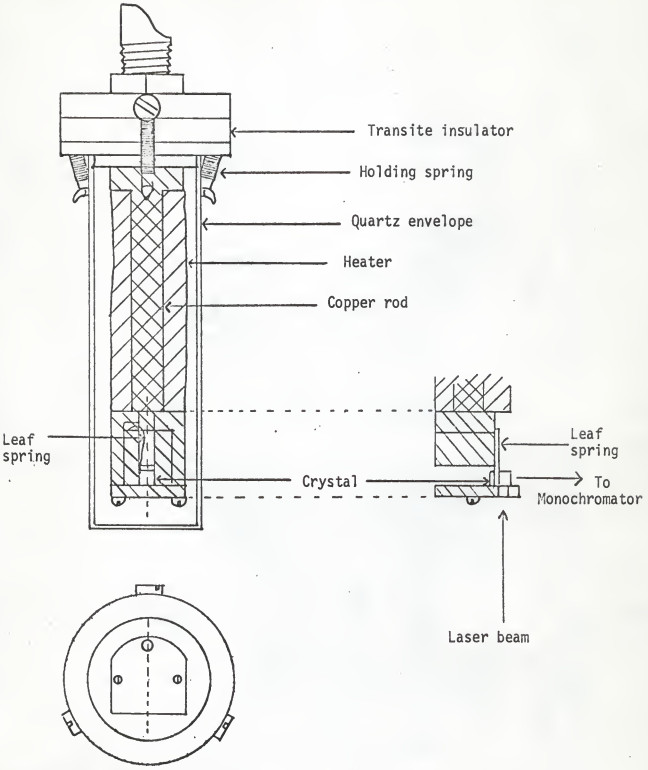
Transite insulator
Holding spring
Quartz envelope
Heater
Copper rod
Leaf spring
Leaf spring
Crystal
To Monochromator
Laser beam

tense Rayleigh scattering. Such minor movement of the crystal caused uncertainty in intensity measurements. The final arrangement was to have the crystal held against one side of the copper block by a light leaf spring. To steady the heater with respect to the laser and monochromator, the adjustments were equipped with lock nuts and the mount was clamped to the lid of the sample box when the crystal was in place.

A problem exists in determining the temperature of the small volume of the crystal from which the data is being taken. A quartz tube was placed around the heater to aid in creating a uniform temperature around the crystal. The thermocouple was placed in contact with the crystal. The recorded temperatures are believed to be accurate to $\pm 2^{o}$ C.

It had been hoped to obtain data to the melting point of the crystal, approximately 250^{o} C (523^{o}K). Between 200^{o}C and 225^{o} C anomalies occurred. In the initial experiments, the crystals shattered. After altering the mount to exert a minimum strain on the crystal, the crystals were found to become translucent to the laser beam. These observations will be discussed in the conclusions.

The low temperature dewar and heater are shown in Plates V and VI. The dewar used liquid nitrogen to cool the crystal. A nichrome wire heater was used to obtain temperatures between 77^{o}K and room temperature. The first heater used only copper. The temperature could not be controlled. A second heater was made with brass between the copper cold finger and the copper platform on which the crystal was mounted. The heater wire was wrapped around the platform. The brass allowed a gradient to be set up and intermediate temperatures to be obtained. The second heater and crystal mount would not cool the crystal below 100^{o}K. A variac was used to control the

EXPLANATION OF PLATE V

A diagram of the dewar and heater used for the studies below room temperature.

PLATE V

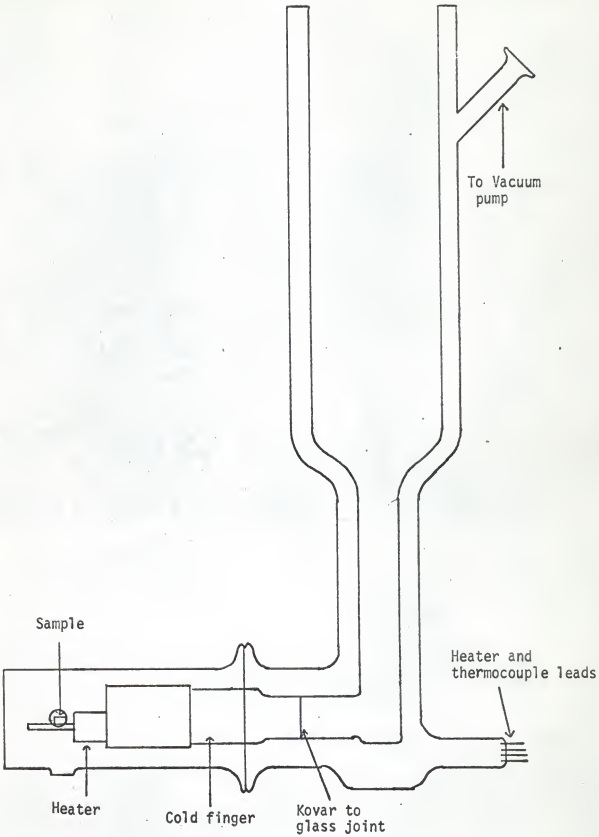
To Vacuum pump
Sample
Heater and thermocouple leads
Heater
Cold finger
Kovar to glass joint

EXPLANATION OF PLATE VI

A close-up diagram of the heater used with the dewar for the low temperature studies.

PLATE VI

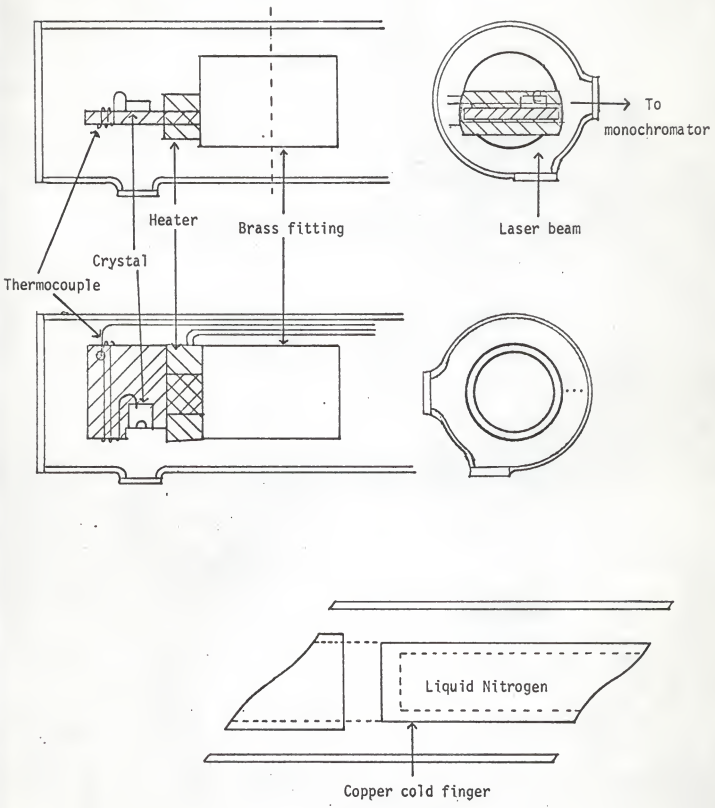
To
monochromator
Laser beam
Heater
Brass fitting
Crystal
Thermocouple
Liquid Nitrogen
Copper cold finger

current to the heater. A suitable platinum resistor and modification of the Athena controller to allow it to operate below $0^{o}C$ would have been an improvement.

A completely satisfactory method of mounting the crystal was not devised. The method used was to hold a large crystal to the platform with conductive grease. Heating and cooling allowed the crystal to move in the grease and thus the usefulness of this mount was limited.

The temperature was monitored by placing an iron-constantan thermocouple on top of the crystal away from the copper platform. Since the heater was in a vacuum, it was assumed that the crystal temperature was uniform since the platform was the only heat sink. The temperature of the cold finger was used as a standard to check on the measured temperatures.

X-ray diffraction from a powder sample of $NaClO_3$ was used to study the variation of the unit cell dimensions with temperature. A camera and heater system built by Babcock[26] was available. The camera had a radius of 6.0 cm. The film jacket was water cooled. The heater, Fig. 8, consisted of a block of Monel metal wrapped with nichrome wire. The rotary mount for the sample extended into a hold through the Monel metal block and the x-rays passed through a slot. The block was suspended from the top of the camera by insulators. The temperature of the sample was monitored by measuring the temperature of the metal block. The calibration of the temperature of the block versus the sample temperature was the main source of error. An attempt to make a more accurate calibration was made by mixing MgO with the sample. The coefficient of thermal expansion of MgO is known. A determination of the temperature could be made by comparing the spectrum superimposed on the $NaClO_3$ spectrum. Although shifts in the $NaClO_3$ lines could be measured,

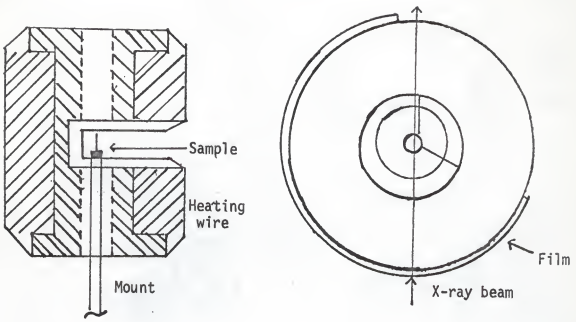

Fig. 8, X-ray Heater

the shift in the MgO lines were too small to be accurately determined over this temperature range. This results from the fact that $NaClO_3$ has an expansion coefficient of 40-70 x $10^{-6}/^{o}C$ while MgO is about 10 x $10^{-6}/^{o}C$. The 720 and 710 planes were used to determine the lattice dimensions of $NaClO_3$. Cobalt K_α radiation was used and available tables[27] were used to determine the spacing from the angle subtended by the lines on the film. The temperature of the heater changed with time and only an average temperature could be recorded.

DISCUSSION OF RESULTS

The temperature variations in the Raman spectral line frequencies and half widths for several phonons of $NaClO_3$ are shown in Plates VII-X. Plate XI shows a typical peak and its shifts for temperatures between 298^{o} K and 496^{o} K. The instrumental spectral slit widths used in these studies are shown in Table I.

Table I

Instrument Slit Widths

Line (cm^{-1})	100-295^{o}K (cm^{-1})	295-450^{o}K (cm^{-1})
76	1.5	2.5
151	1.0	2.5
205	2.5	3.0
487	1.5	---
940	1.0	2.5

The data are presented in a form to allow comparison with the $CaCO_3$ data by Narayanaswang[18]. The data show the same relationship between the frequency shift and half-width changes that was observed in the $CaCO_3$ data. The proportional change of position, χ, also shows striking difference between the internal and external modes as was seen in the $CaCO_3$ data. The values of χ shown in Table II are approximate, but show the difference distinctly. The parameter χ is defined by the relationship

$$\chi = \frac{1}{\nu}\frac{d\nu}{dT} .$$

EXPLANATION OF PLATE VII

A graph of the changes of the 76 cm^{-1} line as a function of temperature. The frequency shift and half-width are plotted versus temperature. A linear least squares fit yields a $0^{o}K$ intercept of 76.0 cm^{-1}, a slope of $-2.92 \times 10^{-2} cm^{-1}/^{o}K$, and a correlation coefficient[29] of -0.96.

PLATE VII

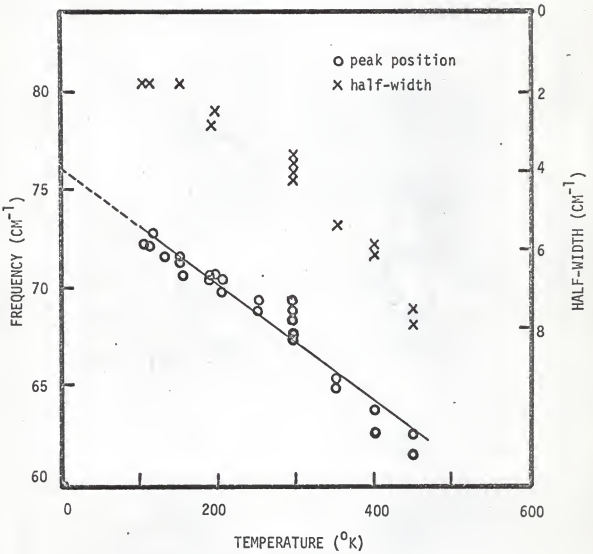
o peak position
× half-width
80
75
70
65
60
0
2
4
6
8
0
200
400
600
FREQUENCY (CM⁻¹)
HALF-WIDTH (CM⁻¹)
TEMPERATURE (°K)

EXPLANATION OF PLATE VIII

A graph of the changes of the 151 cm^{-1} line as a function of temperature. The frequency shift and half-width are plotted versus temperature. A linear least squares fit yields a $0^{o}K$ intercept of 150.6 cm^{-1}, a slope of -5.31×10^{-2} $cm^{-1}/^{o}K$, and a correlation coefficient[29] of -0.98.

PLATE VIII

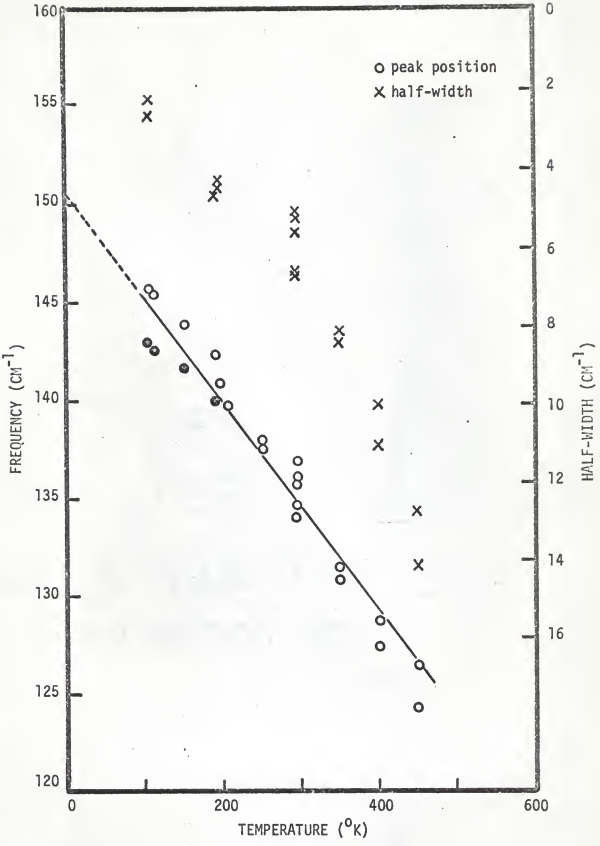
o peak position
× half-width
FREQUENCY (CM^{-1})
HALF-WIDTH (CM^{-1})
TEMPERATURE (^{o}K)
160
155
150
145
140
135
130
125
120
0
2
4
6
8
10
12
14
16
0
200
400
600

EXPLANATION OF PLATE XIX

A graph of the changes of the 205 cm^{-1} line as a function of temperature. The frequency shift and half-width are plotted versus temperature. A linear least squares fit yields a $0^{o}K$ intercept of 205.3 cm^{-1}, a slope of -8.20×10^{-2} $cm^{-1}/^{o}K$, and a correlation coefficient[29] of -0.99.

PLATE IX

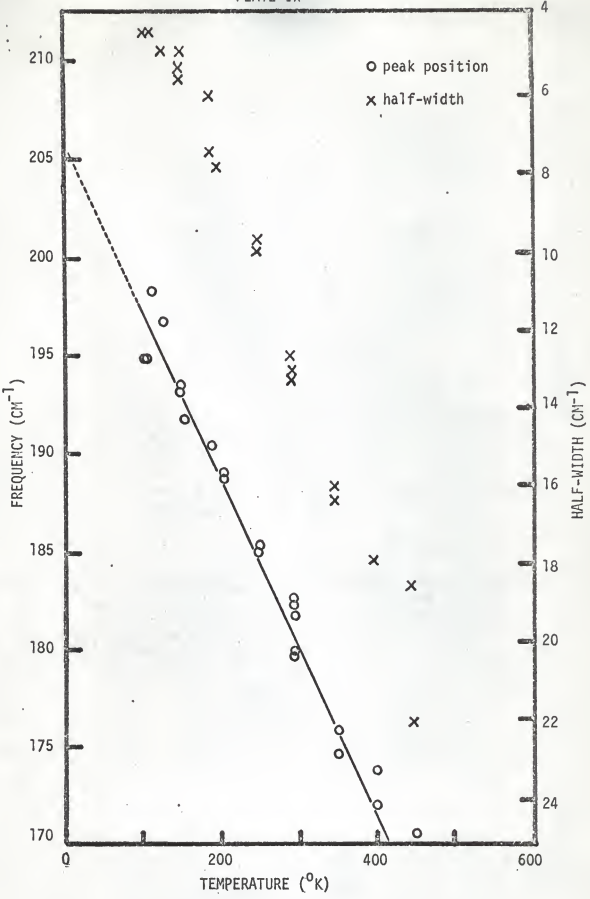
o peak position
x half-width
FREQUENCY (CM^{-1})
HALF-WIDTH (CM^{-1})
TEMPERATURE (^{o}K)
210
205
200
195
190
185
180
175
170
4
6
8
10
12
14
16
18
20
22
24
0
200
400
600

EXPLANATION OF PLATE X

Graphs of the changes of the 487 and 940 cm^{-1} lines as functions of temperature. The frequency shifts and half-widths are plotted versus temperature. A linear least squares fit to the 487 cm^{-1} line yields a $0^{o}K$ intercept of 487.4 cm^{-1}, a slope of -4.18×10^{-3} $cm^{-1}/^{o}K$, and a correlation coefficient[29] of -0.58. A linear least squares fit to the 940 cm^{-1} line yields a $0^{o}K$ intercept of 940.2 cm^{-1}, a slope of -6.78×10^{-3} $cm^{-1}/^{o}K$, and a correlation coefficient of -0.69.

PLATE X

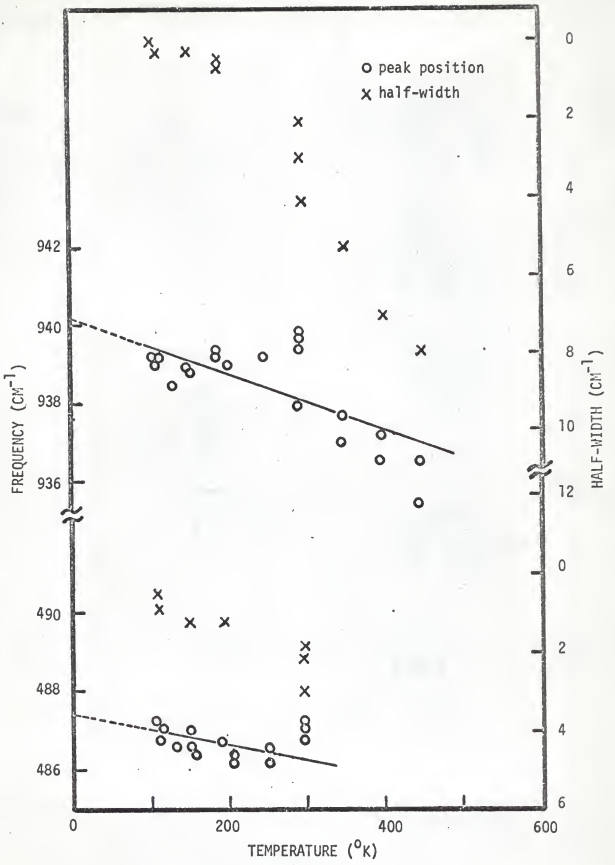
o peak position
x half-width
FREQUENCY (CM^{-1})
HALF-WIDTH (CM^{-1})
942
940
938
936
490
488
486
0
2
4
6
8
10
12
0
2
4
6
0
200
400
600
TEMPERATURE (^{o}K)

EXPLANATION OF PLATE XI

Tracings of the recorder output of five scans of the 151 cm^{-1} line for five temperatures above room temperature.

PLATE XI

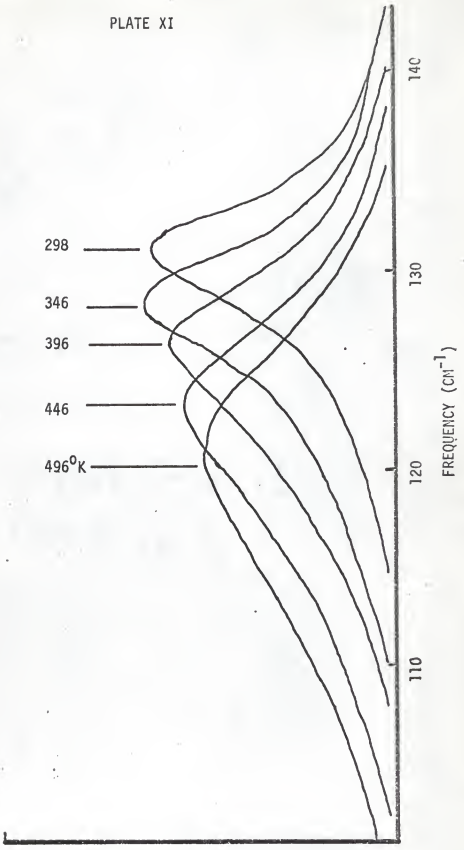

Table II

Proportional change of position of Raman lines in $NaClO_3$

Raman line (cm^{-1})	χ ($/^oC$)
76	$383. \times 10^{-6}$
152	352.
205	399.
487	8.9
940	7.4

Mean values of the data in Plates VII-X are shown in Table III. These are the values to be plotted in the remaining portion of the study. The frequency shift and the values of $\Delta\nu/\nu_o$ are also shown in the table.

The temperature error limits in these studies could not be determined precisely. It was decided to plot the data which was thought to be the most reliable. A limited study comparing the phonons which yielded energy to the incident light to those which took on energy from the incident light, i.e. $\omega_i \pm \omega_R$, showed that the accuracy of determining the peak position was within one wavenumber. This determination was possible because the two Raman shifts are symmetric about the exciting line. The monochromator resolution was usually about 2 cm^{-1}. It is felt that the temperatures in the Raman study are accurate within $\pm 2^oK$ but this could not be verified. The observation that the variation in the measured parameters near room temperature exceeded the values to be expected on the basis of the uncertainties assigned above cannot be explained. The data for the internal modes is not as consistent as the external modes, this probably arises from the relatively small changes in the measured parameters for the internal modes.

TABLE III

Temperature variation of the position and half-width of five Raman lines in $NaClO_3$

Temperature	ν_o = 76 cm^{-1}				ν_o = 151 cm^{-1}				ν_o = 205 cm^{-1}			
(°K)	ν (cm^{-1})	$\Delta\nu$ (cm^{-1})	$\Delta\nu/\nu_o$	$\nu_{\frac{1}{2}}$[a] (cm^{-1})	ν (cm^{-1})	$\Delta\nu$ (cm^{-1})	$\Delta\nu/\nu_o$	$\nu_{\frac{1}{2}}$ (cm^{-1})	ν (cm^{-1})	$\Delta\nu$ (cm^{-1})	$\Delta\nu/\nu_o$	$\nu_{\frac{1}{2}}$ (cm^{-1})
110	72.1	3.9	5.13×10^{-2}	1.8	144.0	6.6	4.38×10^{-2}	2.5	194.9	10.4	5.07×10^{-2}	4.5
128	71.6	4.4	5.79	---	-----	---	----	---	196.7	8.6	4.19	5.0
150	71.5	4.5	5.92	1.8	142.8	7.8	5.18	---	193.3	12.0	5.84	5.4
190	70.6	5.4	7.10	2.9	141.1	9.5	6.31	4.7	190.4	14.9	7.26	6.8
205	70.2	5.8	7.63	---	139.8	10.8	7.17	---	188.8	16.5	8.04	7.9
250	69.2	6.8	8.95	---	137.8	12.8	8.50	---	185.1	20.2	9.84	9.8
295	68.3	7.7	10.13	4.0	135.6	15.0	9.96	5.7	181.1	24.2	11.79	13.0
350	65.2	10.8	14.21	5.4	131.2	19.4	12.88	8.2	175.0	30.3	14.76	16.2
400	53.2	12.8	16.84	6.0	128.2	22.4	14.87	10.6	177.8	32.5	15.83	17.9
450	62.0	14.0	18.42	7.7	125.4	25.2	16.73	13.4	169.0	36.3	17.68	20.3

TABLE III (Cont.)

Temperature variation of the position ahd half-width of five Raman lines in $NaClO_3$

Temperature	ν_o = 487 cm^{-1}				ν_o = 940 cm^{-1}				
(^oK)	ν (cm^{-1})	$\Delta\nu$ (cm^{-1})	$\Delta\nu/\nu_o$	$\nu_{1/2}$ (cm^{-1})	ν (cm^{-1})	$\Delta\nu$ (cm^{-1})	$\Delta\nu/\nu_o$	$\nu_{1/2}$ (cm^{-1})	
110	486.8	.6	1.23×10^{-3}	2.9	939.0	1.2	1.28×10^{-3}	2.3	
128	486.6	.8	1.64	---	938.5	1.7	1.81		
150	486.8	.6	1.23	3.2	939.0	1.2	1.28	2.3	
190	486.8	.6	1.23	3.2	939.3	.9	0.96	2.6	
205	486.3	1.1	2.26	---	939.0	1.2	1.28	---	
250	486.4	1.0	2.05	---	939.2	1.0	1.06	---	
295	487.1	.3	0.62	4.3	939.0	1.2	1.28	5.3	
350	-----	---	----	---	937.4	2.8	2.98	7.1	
400	-----	---	----	---	936.8	3.4	3.62	9.0	
450	-----	---	----	---	936.0	4.2	4.47	10.0	[a]half-width

Several of the lines presented individual problems. Data on the 487 cm^{-1} line was not taken above room temperature because of an oversight. A complication arose when interpreting the high temperature data on the 940 cm^{-1} line. At low temperatures, a second line at 933 cm^{-1} was almost completely resolved and did not affect the peak position or half-width of the 940 cm^{-1} line. But as the temperature increased, the overlap of the two lines increased, until at 450°K, the 933 cm^{-1} line is not separately observable. When possible, the two lines were deconvoluted, but at higher temperatures, the half-width of the 940 cm^{-1} line included the 933 cm^{-1} line. A similar problem occurred with the 151 cm^{-1} line. At very low temperatures, two peaks could be seen quite distinctly, but above 200°K, only one peak could be observed. The two lines at low temperature were treated as variations of the same point, although the higher frequency line seems to be a better continuation of the higher temperature data. At intermediate temperatures, i.e. 150°K, the half-widths had no meaning as the two peaks could not be resolved, but above 200°K, the half-width data is as consistent as the data on other Raman lines. The 76 cm^{-1} line was the only line seriously affected by the Rayleigh scattered radiation. In the data presented, the influence of the Rayleigh scattered line was easily removed.

It had been hoped to work near the melting point of $NaClO_3$, 525°K (252°C). However the crystal became translucent at approximately 475-500°K. It is thought possibly the ClO_3^- ion became sufficiently free rotating at its lattice site that the disorder in the crystal was increased greatly. Deshpande and Mudholker[28] report a splitting in the X-ray diffraction lines above 200°C but they do not explain this. They use the average of the two lines and the measured parameters continue the smooth curve from lower

temperatures to obtain lattice parameters at high temperatures. As the temperature increased, the 205 cm^{-1} line became extremely broad, until at 450°K it was barely resolvable from the background. Narayanaswamy[18] states that the 281 cm^{-1} line in $CaCO_3$ is due to a hindered rotation of the $CO_3^=$ ion about its axis, and it would appear that the 205 cm^{-1} line in $NaClO_3$ corresponds to the same type of motion. A very poor Raman spectrum taken at a temperature above the change shows that the strong Raman lines are still present. Thus the Raman data and the x-ray data seem to agree that there has been no structure change, and do indicate the possibility that the ClO_3^- ion is allowed to rotate freely at high temperatures.

The data presented in Plates VII-X approximate straight lines over the temperature range studied. This is in contradiction to the data on $NaClO_3$ presented by Kumari[20]. Above room temperature his data does approach straight lines, but the present study would indicate that his temperature measurements below room temperature are much too low. The numerical values of the frequency show some disagreement, while the shift in frequencies of the 76 and 151 cm^{-1} lines are in agreement. The 205 cm^{-1} data shows twice the shift Kumari reports. Kumari was unable to detect a shift in the 487 and 940 cm^{-1} lines. A straight line was fit to each set of frequency shifts reported in Plates VII-X. The slope, intercept, and correlation coefficient[29] of the least squares fits are also reported in Plates VII-X.

Most theories of anharmonicity require the use of the harmonic oscillator model parameters. Therefore, it is of interest experimentally to know approximate harmonic frequency values. The harmonic approximation would achieve its best agreement with experimental results at 0°K. This temperature cannot be achieved experimentally, but an extrapolation of

higher temperature values can be made. The extrapolated $0^{o}K$ value was used because it was closer to the harmonic value than a value at any other temperature. For example, the quantity $\Delta\nu/\nu_o$ was used in this study, where ν_o should be the harmonic oscillator frequency, ν_h. If the error in the value of ν_h is δ, the quantity can be written

$$\frac{\Delta\nu}{\nu_h} = \frac{\Delta\nu}{\nu_o+\delta}$$

$$= \frac{\Delta\nu}{\nu_o}\left(1 + \frac{\delta}{\nu_o}\right)^{-1} \qquad (29)$$

$$= \frac{\Delta\nu}{\nu_o}\left(1 - \frac{\delta}{\nu_o} + \cdots\right),$$

if δ is much less than ν_o. Eq. (29) can be rewritten

$$\frac{\Delta\nu}{\nu_h} = \frac{\Delta\nu}{\nu_o} - \Delta\nu\frac{\delta}{\nu_o^2} + \cdots \quad . \qquad (30)$$

Thus when a harmonic value is needed, the extrapolated value should be used even if it is a poor approximation.

The x-ray diffraction data of the unit cell dimensional variation with temperature is shown in Plate XII. Data from a study by Deshpande and Mudholker[28] also are included with the present data. The agreement between the two studies is very close considering the uncertainty in the X-ray temperature calibration. Deshpande does not list any uncertainty for his measurement. The values from the present study are only 10% accurate. Equipment to continue the x-ray study below room temperature was not available and no reports on this could be found in the literature. Plate XIII shows that over the temperature range studied, the volume is essentially

EXPLANATION OF PLATE XII

A graph of the lattice parameter versus temperature for the cubic $NaClO_3$ unit cell. The data was obtained with x-ray diffraction from powdered samples. The values from the present study and the values obtained by Deshpande and Mudholker[28] are both plotted.

PLATE XII

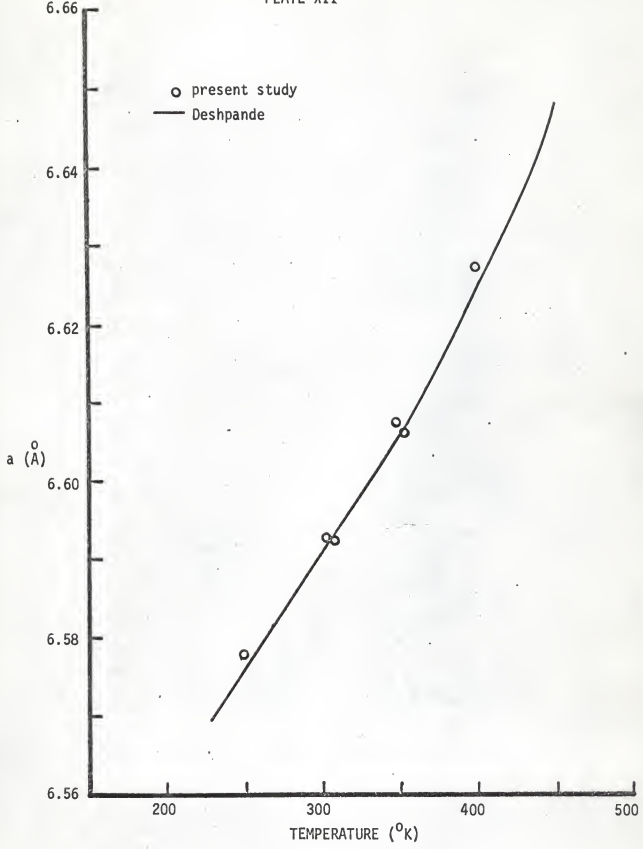
6.66
6.64
6.62
6.60
6.58
6.56
a (Å)
o present study
Deshpande
200
300
400
500
TEMPERATURE (°K)

EXPLANATION OF PLATE XIII

A graph of the volume of the $NaClO_3$ unit cell versus temperature. The value at 250°K is an extrapolated value using a least squares fit to the data. The linear least squares fit yields a 0°K intercept of 271.9 $\mathring{A}^3$, a slope of 4.14×10^{-2} $\mathring{A}^3/°K$ and a correlation coefficient[29] of 0.998.

PLATE XIII

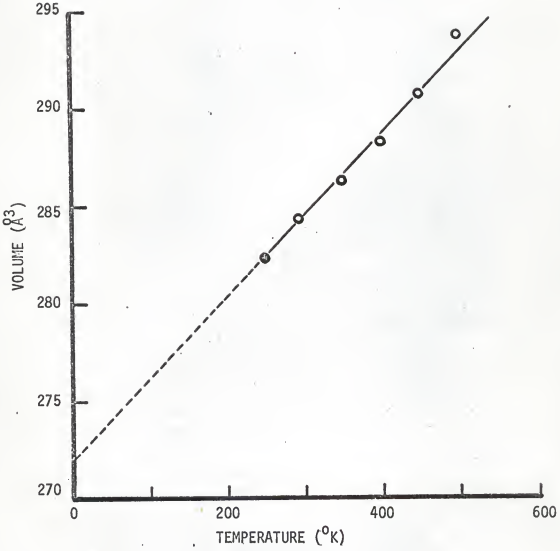

a linear function of temperature.

Plates XIV and XV present the data of both Raman and x-ray experiments in a form relevant to Eq. (16),

$$\frac{\Delta\nu}{\nu} = -\gamma\frac{\Delta V}{V} \quad . \tag{16}$$

As with the frequencies, the harmonic model volume was assumed to be given by an extrapolation to $0^{o}K$. The lack of volume data below room temperature greatly limits the completeness of the graph. It was felt that the volume could be extrapolated to $250^{o}K$ with some accuracy and it seems to fit the other data. Grüneisen's "constant", γ, is the slope of the curve at any given point. It would appear that γ is essentially the same for the three external modes, but it appears that γ is not constant over this temperature range. The 940 cm^{-1} line, an internal mode, shows the same characteristics but different values of γ. See Plate XV.

The data is presented in Plates XVI and XVII in a form convenient to compare with Eq. (19),

$$\frac{\Delta\nu}{\nu} = -3\alpha\gamma\Delta T. \tag{19}$$

The straight line formed by the data in Plate XVI is quite striking since α and γ are thought to be functions of temperature. The slope of a straight line is a constant and thus $(-3\alpha\gamma)$ is a constant. Refering to Eq. (20),

$$\frac{\partial \ln\theta}{\partial T} = -3\ \alpha\gamma, \tag{20}$$

it is thus seen that the change in the Debye temperature over this temperature range is a constant. The studies reported by Blackman[30] supports this result that θ can be a linear function of temperature at temperatures above approximately $100^{o}K$. A least squares fit to the data presented in Plate XVI

EXPLANATION OF PLATE XIV

A graph of $\Delta\nu/\nu_0$ versus $\Delta V/V_0$ for the 76, 151, and 205 cm^{-1} lines. The temperature of each point plotted is indicated at the top of the graph.

PLATE XIV

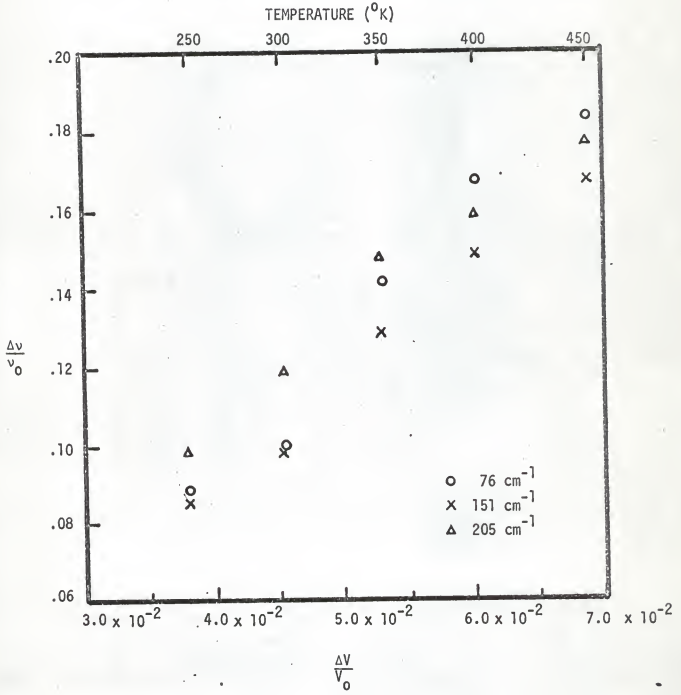
TEMPERATURE (°K)
250
300
350
400
450
.20
.18
.16
.14
.12
.10
.08
.06
Δν/ν₀
3.0 x 10⁻²
4.0 x 10⁻²
5.0 x 10⁻²
6.0 x 10⁻²
7.0 x 10⁻²
ΔV/V₀
76 cm⁻¹
151 cm⁻¹
205 cm⁻¹

EXPLANATION OF PLATE XV

A graph of $\Delta\nu/\nu_0$ versus $\Delta V/V_0$ for the 487 and 940 cm^{-1} lines. The temperature of each point plotted is indicated at the top of the graph.

PLATE XV

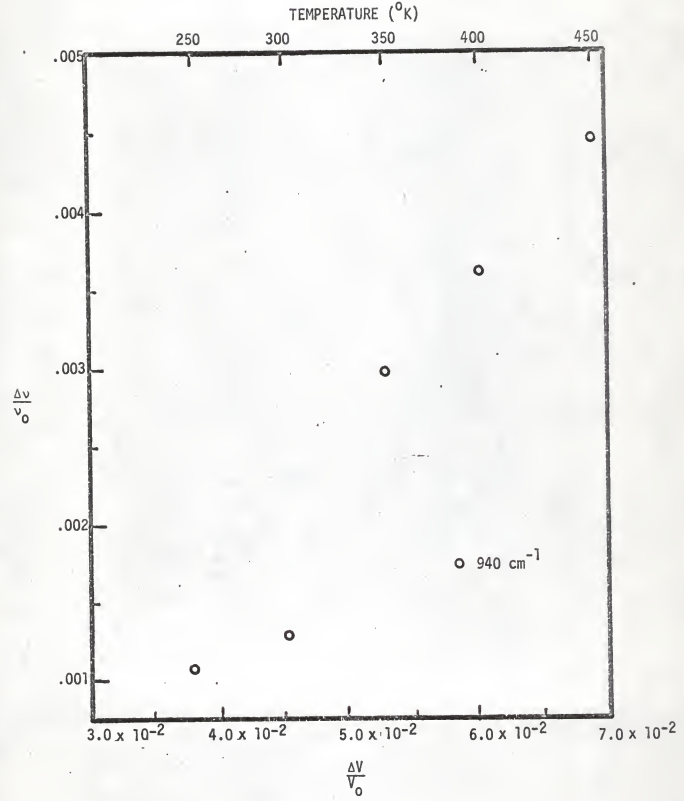
TEMPERATURE (°K)
250
300
350
400
450
.005
.004
.003
.002
.001
$\frac{\Delta\nu}{\nu_o}$
940 cm^{-1}
3.0 x 10^{-2}
4.0 x 10^{-2}
5.0 x 10^{-2}
6.0 x 10^{-2}
7.0 x 10^{-2}
$\frac{\Delta V}{V_o}$

EXPLANATION OF PLATE XVI

A graph of $\Delta\nu/\nu_0$ versus temperature for the 76, 151, and 205 cm^{-1} lines. A linear least squares fit yields a $0^{o}K$ intercept of -1.32×10^{-3}, a slope of $3.84 \times 10^{-4}/^{o}K$, and a correlation coefficient[29] of 0.97.

PLATE XVI

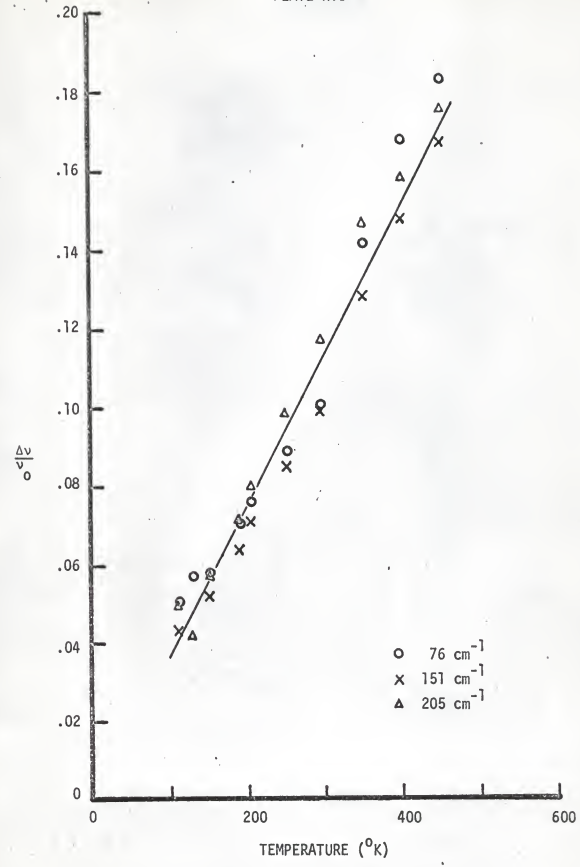
.20
.18
.16
.14
.12
.10
.08
.06
.04
.02
0
$\frac{\Delta\nu}{\nu_o}$
0
200
400
600
TEMPERATURE (°K)
76 cm^{-1}
151 cm^{-1}
205 cm^{-1}

EXPLANATION OF PLATE XVII

A graph of $\Delta\nu/\nu_0$ versus temperature for the 487 and 940 cm^{-1} lines. A linear least square fit yields a $0^{o}K$ intercept of -3.46×10^{-5}, a slope of $7.24 \times 10^{-6}/^{o}K$, and a correlation coefficient[29] of 0.64.

PLATE XVII

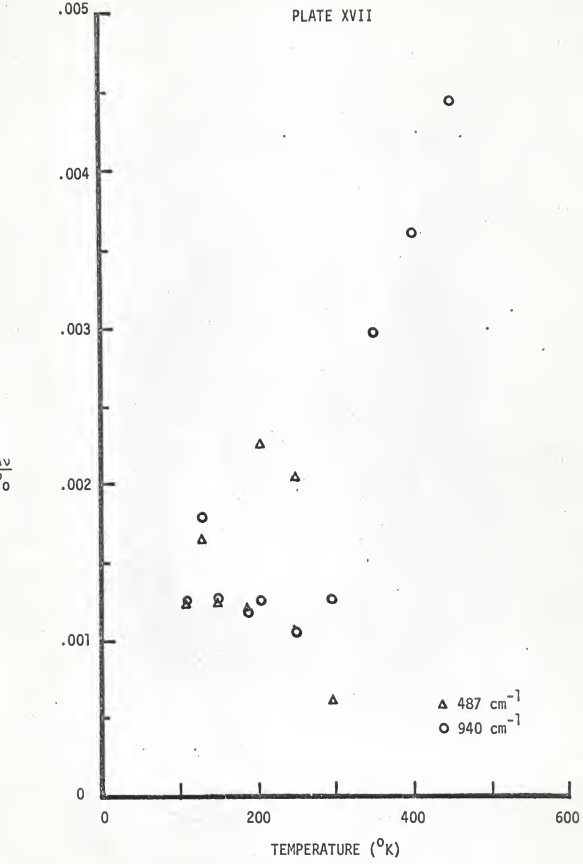
.005
.004
.003
.002
.001
0
$\frac{\Delta\nu}{\nu_o}$
0
200
400
600
TEMPERATURE (°K)
Δ 487 cm^{-1}
O 940 cm^{-1}

EXPLANATION OF PLATE XVIII

A graph of the half-width versus $(T/V)^{\frac{1}{2}}$ for the four lines studied above room temperature.

PLATE XVIII

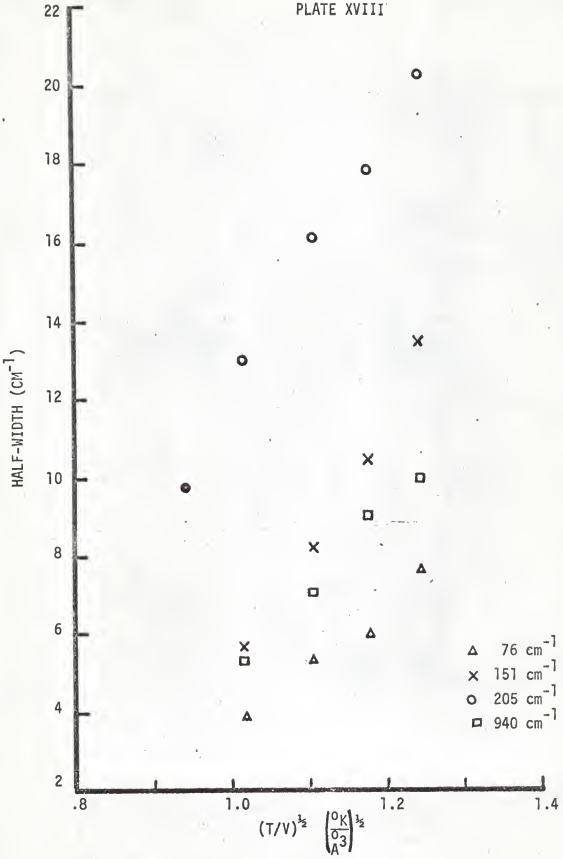
HALF-WIDTH (CM^{-1})
22
20
18
16
14
12
10
8
6
4
2
.8
1.0
1.2
1.4
$(T/V)^{\frac{1}{2}}$ $\left[\frac{^{o}K}{^{o}A^{3}}\right]^{\frac{1}{2}}$
76 cm^{-1}
151 cm^{-1}
205 cm^{-1}
940 cm^{-1}

gives a value of $(-3\alpha\gamma) = 3.84 \times 10^{-4}/^{o}K$ and to the data in Plate XVII, $(-3\alpha\gamma) = 5.97 \times 10^{-6}/^{o}K$.

When the graphs in Plates VII to X were drawn straight lines were not expected for the frequency shifts. A little thought will show that they are essentially the same as the graphs in Plates XVI and XVII. The constant ν_0 was left out, and therefore the slopes are different.

The relationship of the data to the theoretical expression of Eq. (15) is not known,

$$h\Delta\nu = \sum_i \beta_i \left[\exp(h\nu_i/kT)-1\right]^{-1} . \qquad (15)$$

Equation (15) predicts a straight line at high temperatures, but $200^{o}K$ is usually not considered a high temperature.

Not many conclusions can be drawn from the half-width data. A plot of $(T/V)^{\frac{1}{2}}$ versus the half-width, $\nu_{\frac{1}{2}}$, is shown in Plate XVIII. The result is not a straight line, but since the temperature dependence of the compressibility, β, was ignored, the results are very good and seem to verify Eq. (21).

$$\nu_{\frac{1}{2}} \propto \left(\frac{kT\beta}{V}\right)^{\frac{1}{2}} \qquad (21)$$

At low temperatures the monochromator resolution was of the same order of magnitude as the half-widths. This caused distortion of the half-width values. The half-width as a function of monochromator resolution is shown in Appendix A.

Summary and Conclusions

The study of the temperature dependence of the Raman spectrum of $NaClO_3$ allows several conclusions to be drawn. A simple Grüneisen law seems adequate to describe the relation between the frequency and volume. The

frequency shifts appear to be linear with temperature and this requires that the product of the coefficient of expansion and the Grüneisen constant to be a constant, while both are individually functions of temperature. This product of the coefficient of expansion and Grüneisen's constant is proportional to the change of the Debye temperature with temperature and this indicates that the change in constant over the temperature range studied. The vibrations seem to group themselves into two classifications, external and internal modes. It also appears that if one allows changes of compressibility with temperature, the half-width can be described by a simple statistical model.

The study can be improved and extended in several directions. The first need is to extend the lattice dimension study below room temperature. It would be worthwhile to study other modes of vibration to see if they confirm the conclusions of the present study. The most straight forward manner of proceeding would be to repeat the Raman study with a better monochromator. This would allow for greater resolution and an improved signal to noise ratio. With this monochromator, meaningful data could be taken at the other polarizations allowing study of additional vibrations, particularly internal modes. The study could be made with the heater in the dewar being able to reach the higher temperature. This might remove the discontinuity at room temperature. It became apparent during the study that when scanning a region containing several peaks of various heights a recorder with a logarithmic presentation would be useful to present the weaker peaks more clearly.

Most models of solids consider the force between atoms to be a function of the distance between the interacting atoms. Most models of solids, also consider the frequency with which an atom vibrates about its equilibrium

position in the lattice to be a function of the force between interacting atoms. Thus it would appear that the frequency with which an atom vibrates should be a function of the distance between interacting atoms. It is interesting therefore, that as simple a law as Grüneisen's would be followed so closely. In a cubic crystal, it is possible that all of the ionic bonds expand uniformly. Since the covalent bonds will respond to temperature in a different manner, the corresponding vibrations should also behave differently. Two possible studies seem suggested. The simpler one would be to repeat the present study with crystals having symmetries other than cubic. Probably orthorhombic or tetragonal would be the simplest to interpret. The second approach would be to repeat the study on materials for which the lattice vibration assignments and bond length changes as functions of the temperature are known. Considerable work is needed before such data is available. But the bond lengths and vibration frequencies are two of the basic properties of solids and understanding any relationships between them would greatly aid in understanding solids in general. Both are properties of the potential energy field existing inside the solid and thus such studies are attempts to understand this potential. Both suggested studies should be on materials containing strong ionic and covalent bonds. At this stage of understanding, hybrid bonding in the materials studied would probably make interpretation more difficult.

Appendix A

A study of the half-width, the 487 cm^{-1} peak, as a function of monochromator resolution is shown in Plate XIX. Although the uncertainties are large, for small resolution, the half-width is approximately a constant as the resolution changes. When the spectral slit width increases above about 66% of the constant value of the half-width, the half-width begins to increase with increasing spectral slit width. Thus when the resolution is much smaller than the measured half-width, the half-width is close to its constant value.

EXPLANATION OF PLATE XIX

A graph of the measured half-width versus monochromator spectral slit width. The 487 cm^{-1} line was studied at 104 and 295^{o}K to provide two different phonon half-width values.

PLATE XIX

× 104°K
o 295°K
HALF-WIDTH (CM⁻¹)
MONOCHROMATOR SPECTRAL SLIT WIDTH (CM⁻¹)
0
2
4
6
8
1.0
2.0
3.0
4.0
5.0

ACKNOWLEDGEMENTS

The author wishes to acknowledge and thank Dr. Charles E. Hathaway for his guidance and assistance in this study. He also wishes to thank Dr. R. Dean Dragsdorf for his assistance in the x-ray portion of the study. Mrs. Indira Nair has given much helpful advice and counsel. The author also wishes to thank Mrs. Nair and George Simonis for growing the crystals used in the study and the Department of Defense Themis Program (Office of Naval Research) for financial assistance.

REFERENCES

1. I. Newton, Principia, Book II (1686).
2. M. Born and K. Huang, Dynamical Theory of Crystal Lattices (Clarendon Press, Oxford, 1956).
3. L. Brillouin, Wave Propagation in Periodic Structure (Dover Publications, Inc., New York, 1953), 2nd ed.
4. G. Mie, Ann. Physik [4] 11, 657 (1903).
5. E. Grüneisen, Ann. Physik [4] 26, 393 (1908).
6. G. Leibfried and W. Ludwig, Solid State Physics (Academic Press, New York, 1961), vol. 12, p 275.
7. G. Leibfried, Lattice Dynamics (Pergamon Press, Oxford, 1963), p. 237.
8. H. Goldstein, Classical Mechanics (Addison-Wesley Publishing Company, Inc., Reading, 1965), p. 318.
9. C. Kittel, Introduction to Solid State Physics (John Wiley and Sons, Inc., New York, 1966), 3rd ed., p. 109.
10. C. V. Raman and K. S. Krishnan, Nature 121, 501 (1928).
11. R. Loudon, Adv. Phys. 13, 423 (1964).
12. I. Nair, Thesis, Kansas State University (1969).
13. A. A. Maradudin, A. E. Fein, and G. H. Vinegard, Phys. Stat. Sol. 2, 1479 (1962).
14. K. S. Viswanathan, Can. J. Phys. 41, 423 (1963).
15. K. S. Viswanathan, Proc. Indian Acad. Sci. A 47, 405 (1958).
16. J. M. Ziman, Electrons and Phonons (Clarendon Press, Oxford, 1960), p. 418.
17. C. Aravindakshan, Z. Krist, 111, 241 (1959).

18. P. K. Narayanaswamy, Proc. Indian Acad. Sci. A 26, 511 (1947).

19. C. S. Kumari, Proc. Indian Acad. Sci. A 32, 177 (1950).

20. C. S. Kumari, Proc. Indian Acad. Sci. A 31, 348 (1950).

21. Spex Industries, Inc., "Ramanlogs" 1, No. 2 (1968).

22. G. B. Benedek and K. Fritsch, Phys. Rev. 149, 647 (1966).

23. J. J. Barrett and N. I. Adams, J. Opt. Soc. Am. 58, 311 (1968).

24. F. A. Jenkins and H. E. White, Fundamentals of Optics (McGraw-Hill Book Company, Inc., New York, 1957), 3rd ed., p. 344.

25. V. Ananthanarayanan, Z. Physik, 159, 51 (1960).

26. E. R. Babcock, Thesis, Kansas State University (1950).

27. "Tables for Conversion of X-ray Diffraction Angles to Interplaner Spacings," AMS 10, National Bureau of Standards (1950).

28. V. T. Deshpande and V. M. Mudholker, Acta Cryst. 13, 483 (1960).

29. J. E. Freund, Mathematical Statistics (Prentice-Hall, Inc., Englewood Cliffs, N.S., 1962).

30. M. Blackman, Handbuch der Physik (Springer-Verlag, Berlin, 1955), Vol. VII, Part 1, p. 325.

TEMPERATURE VARIATION OF RAMAN SPECTRUM OF SODIUM CHLORATE

by

HARVEY LAWRENCE JOHNSTON, JR.

B. S., University of Missouri, 1967

AN ABSTRACT OF A MASTER'S THESIS

submitted in partial fulfillment of the

requirements for the degree

MASTER OF SCIENCE

Department of Physics

Kansas State University
Manhattan, Kansas

1969

ABSTRACT

A laser Raman spectrometer has been constructed. The system includes an optimized focused geometry for illuminating the sample and collecting the scattered radiation. This system has been used to study the variation of the frequencies and half-widths as a function of temperature (100 to 450°K) of five lines in the Raman spectrum of a sodium chlorate single crystal. The 68, 134, and 180 cm^{-1} lines represent vibrations involving relative motion of the sodium and chlorate ions, while the 486 and 938 cm^{-1} lines represent vibrations involving only internal motions of the chlorate ion. A simple form of Grüneisen's law seems adequate to describe the variation of the frequency as a function of volume. It was found that the product of the coefficient of expansion and the Grüneisen constant was constant over the temperature range studied. This implies that the logarithm of the Debye temperature is a linear function of temperature. The Grüneisen constant for the low frequency vibrations was found to be quite different from the constant for the chlorate vibrations. If one allows for variation of compressibility with temperature, a general description of the half-width variation can be described by a simple statistical model.